The International Journal of Advanced Manufacturing Technology (2018) 99:937–949
https://doi.org/10.1007/s00170-018-2451-6

ORIGINAL ARTICLE

An identification model of cutting force coefficients for five-axis ball-end milling

Minglong Guo[1] · Zhaocheng Wei[1] · Minjie Wang[1] · Shiquan Li[1] · Shengxian Liu[1]

Received: 8 February 2018 / Accepted: 17 July 2018 / Published online: 15 August 2018

Abstract
Five-axis ball-end milling is widely used in energy, ship, aerospace, and other fields. As one of the difficulties in milling research, milling force is often critical to the processing efficiency and quality of part. For predicting the milling force of the five-axis ball-end milling better, this paper presents a cutting force coefficients identification model which is related to the instantaneous chip layer thickness and axial position angle considering the cutter run-out. For five-axis ball-end milling of the oblique plane, the relationship of feed direction, cutter axis vector, and machined surface is parameterized. The boundary curves of cutter workpiece engagement (CWE) are determined by intersecting spatial surfaces. The boundary curves are discretized, and an algorithm of in-cut cutting edge (ICCE) is proposed by defining the distance between discrete points and the cutting edge. Combining the instantaneous chip thickness considering arbitrary feed direction and cutter run-out, the five-axis milling force model of ball-end mill is established. Based on the undetermined coefficient method and the instantaneous average milling force of teeth, the cutting force coefficients identification model corresponding to the instantaneous chip layer thickness and the axial position angle is established. Furthermore, cutter run-out parameters are obtained combined with instantaneous measured milling force of single tooth. The experimental and simulation examples demonstrate that the CWE determined by the spatial surfaces is consistent with the experimental results. The ICCE is in good agreement with the simulation results based on the solid modeling method. A large number of milling experiments under different processing parameters show that the cutting force coefficients and cutter run-out parameters identification model can be effectively applied to five-axis ball-end milling.

Keywords Ball-end mill · Five-axis milling · CWE · ICCE · Cutting force coefficients · Cutter run-out

1 Introduction

Five-axis ball-end milling occupies an important position in the complex surface manufacturing of aerospace, energy, mold, and other areas. The high efficiency and high precision milling have always been the goal pursued by the industry. Milling force, as one of the most important physical parameters, directly affects tool wear, workpiece deformation, and machining vibration. It is very important for developing a reliable and effective machining plan which is the focus of milling dynamics research. The key elements of milling force model are determining the cutter workpiece engagement (CWE) and identifying cutting force coefficients accurately. In five-axis milling process simulation, the shape of the workpiece surface is complex; the cutter feed direction and cutter axis vector are constantly changing. All of these lead to the change of CWE, as well as the change of in-cut cutting edge (ICCE), namely the cutting edge interval with cutting material. The cutting force coefficients of ball-end mill vary with the axial angle due to the change of the helix angle. According to Zhang et al.'s theory [1], the cutting force coefficients are related to the instantaneous chip layer thickness because of its size effect. In addition, the rotation center does not coincide with the geometric center, namely the cutter run-out [2], which changes the distribution of the chip thickness between the teeth and has an important effect on the peak of the milling force waveform.

At present, most of the ball-end milling force prediction in literatures focus on three-axis. Although several researches for five-axis machining have been introduced in literatures, there

✉ Zhaocheng Wei
wei_zhaocheng@dlut.edu.cn

[1] Key Laboratory for Precision and Non-traditional Machining Technology of Ministry of Education, Dalian University of Technology, Dalian 116024, People's Republic of China

is room for improvement. When studied the five-axis ball-end milling force prediction on the basis of Z-map discretization method, Guo et al. [3] divided the geometry characterizes of the machining parts into grids, then argued that the micro-cutting edge is involved in cutting if the two criteria conditions are met: one is the micro-cutting edge below constraint plane, and the other is the projective point within the projection of grid. Fussell et al. [4] represented the workpiece with Z-buffers elements. The swept envelope of the tool path in five-axis machining is transformed approximately by the three-axis swept envelope of tool path. The CWE was obtained from workpiece and swept envelope. Furthermore, for the milling force prediction with large axial cutting depth, the ICCE of ball-end milling was determined. Based on semi-discrete solid modeling method, the removal volume obtained from intersection of tool swept envelope and workpiece was discretized into thin layers, and then the tool-slice intersection curves can be obtained via two-dimensional intersection operation between the thin layers and tool geometry. Ultimately, Ferry et al. [5] established a CWE model for five-axis flank milling of conical ball-end mill by combining 2D Boolean operation with tool swept area. Boz et al. [6] developed solid modeling method for solving CWE of five-axis ball-end milling based on Parasolid software. Then, the ball-end milling cutter was divided into a series of thin layers along the axial direction in the plane perpendicular to cutter axis and the cutting in angle and the cutting out angle of each cutting thin layer were obtained. Thereby, the milling force prediction of the curved surface machining was realized. The limitation of the contact area obtained by the discrete method and the solid method is that the efficiency and accuracy cannot be taken into account at the same time, which makes them difficult to apply to the five-axis machining of large complex surfaces. Ozturk et al. [7] established a milling force prediction model considering the inclination angle for the ball-end mill slot machining, thereupon regarding ball-end milling of sculptured surface, and proposed an analytical CWE model where front lean angle is considered [8]. Sun et al. [9] judged the cutting condition of a cutting edge element by evaluating whether the cutting edge element is located in the bounding box of workpiece and out of former cutting edge swept surface or not. Whereafter they established milling force prediction model of five-axis ball-end milling. Regarding five-axis ball-end milling of complex surface, Wei et al. [10] transformed five-axis milling considering arbitrary feed direction and cutter axis vector into three-axis milling to evaluate analytical CWE based on layered discretization thought. This method conforms to the five-axis machining characteristics, but the research is limited to the CWE. It did not give effective ICCE algorithm.

Cutting force coefficient identification is an important part of mechanical cutting force model. There are many relevant researches. Based on Armarego's classical oblique cutting model, Lee et al. [11] started with the theoretical formula of coefficients and obtained yield shear stress, shear angle, and other parameters by a series of orthogonal cutting experiments to identify the coefficients. Kim et al. [12] defined the cutting force as the product of cutting force coefficients, the mth power of chip thickness, and the width of the chip layer. The cutting force coefficients are cubic polynomial of axial position angle and m reflects the size effect. Considering the cutting force coefficients as 6 constants, Wang et al. [13] presented an analytical method of cutter run-out parameters identification based on the force model of three-axis slot cutting of ball-end mill. Considering the shear force coefficients as the polynomial of axial height z and the plow force coefficients as constants, Lamikiz et al. [14] established a cutting force coefficients identification model. They studied and compared the linear, quadratic, and cubic shear force coefficients in this model. The above cutting force coefficients are all based on the horizontal machining where the cutter axis is vertical. In order to explore the relationship between the coefficients and the axial position angle, the axial cutting depth is often very large. Cao et al. [15] carried out the cutting coefficients identification experiments that front lean angle existed. The shear force coefficients and the plow force coefficients in the three directions were regarded as constants. The cutting force coefficients corresponding to the different ranges of axial position angle were obtained by changing the front lean angle. Regarding ball-end milling of cylinder part, Yao et al. [16] proposed the plow force coefficients as the polynomial of axial position angle, shear force coefficients as the product of the polynomial of axial position angle, and the polynomial of instantaneous chip thickness. Then, the cutter run-out was further determined by finding the critical condition where the instantaneous chip thickness was zero. Dividing the ball region of ball-end mill into thin disks, Lazoglu et al. [17] designed horizontal slot cutting experiments with thin workpiece which assumed only one disk was in engaged with the workpiece, and then estimated the coefficients of thin disks corresponding to different axial heights. Regarding ball-end slot finishing milling of inclined surface, Szymon et al. [18] obtained the shear and plow force coefficients assumed polynomial of inclination angle considering cutter run-out. Cutter run-out was measured by incremental displacement transducer, and the influence of feed engagement on coefficients was discussed. Li et al. [19] regarded shear force coefficients as the n times polynomial of axial position angle, plow force coefficients as constants. They calibrated cutting force coefficients combining instantaneous milling force and least square method in multi-axis ball-end milling. At present, there are many kinds of cutting force coefficient models and identification experimental methods for ball-end mill. However, cutting force coefficients considering the cutter run-out, the axial position angle, and the instantaneous chip thickness need to be further studied to better adapt to the five-axis machining.

Chattering phenomena in milling experiments should be avoided in identification of cutting force coefficients, especially considering cutter run-out. The deformation of the cutter deflection caused by the chatter can be avoided when cutting system is in a stable state, thus ensuring the accurate correspondence between the instantaneous chip thickness and the cutting force coefficients, as well as the consistency between the definition of the run-out parameters and the actual milling experiment. Recently, Wan et al. [20–23] have done some theoretical research on the stability analysis of milling dynamics. Based on the semi-discrete time domain algorithm [20], lowest envelop method was proposed to obtain the stability field lobe diagram combining multi-order mode of the milling system. In [21], the mechanism of dynamic and static cutting was studied. In the research, the relationship between plowing force and the materials extruded under the clearance face of cutter was expressed by a unified proportional function. A new method to obtain the process damping from the stabile milling experiment was proposed in [22], and the precision of the milling stability diagram based on the process damping was improved. For the thin-walled part with weak rigidity [23], additional mass was added to the workpiece to change the modal parameters, achieving the maximum material removal rate by improving the cutting stability. The above researches on the dynamics analysis of milling system is of guiding significance for selecting reasonable machining parameters in the identification of cutting force coefficients.

Regarding instantaneous milling force of non-slot experiment, a cutting force coefficient identification model relative to instantaneous undeformed chip thickness and axial position angle considering cutter run-out is proposed. General idea of this paper is shown in Fig. 1. Five-axis machining of inclined plane taken as studying subject, the arbitrary relationship of feed direction, cutter axis, and workpiece surface is parameterized. The boundary curves and endpoints of CWE are obtained using spatial surface intersection. Through the discretization of the boundary curves, the endpoints of ICCE on cutting edge are searched. Furthermore, the five-axis ball-end milling force model of inclined plane is established by combining micro-cutting force model and instantaneous chip thickness considering cutter run-out, arbitrary feed direction, and cutter axis direction. The cutting force coefficients can be calibrated using undetermined coefficients method by bringing measured instantaneous average milling force of teeth into milling force model. Then, discrete coefficients related to axial position angle and instantaneous chip thickness are fitted with surface. Then, cutter run-out parameters are solved by combining the coefficients with measured instantaneous milling force of single tooth.

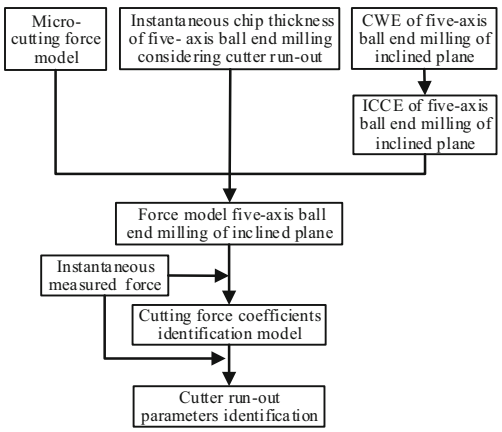

Fig. 1 General idea

2 Force model of five-axis ball-end milling

The five-axis machining with ball-end mill of inclined is shown in Fig. 2. The relationship between the cutter axis, the feed direction, and the inclined plane is arbitrary. The center of the ball-end mill is defined as the origin O of the cutter coordinate system $O\text{-}X_cY_cZ_c$. The vector $\boldsymbol{p}$ along the cutter axis is the Z_c axis. The cross product vector $\boldsymbol{s}$ from vector $\boldsymbol{p}$ to normal vector $\boldsymbol{n}$ of oblique plane is X_c axis. Y_c axis is determined with the rule of right-hand coordinate system. In order to describe the relative position of cutter axis and feed direction $\boldsymbol{f}$, the angle between the cutter axis and the normal vector $\boldsymbol{n}$ is defined as cutter inclination angle ε. The angle between the X_c axis and the feed direction $\boldsymbol{f}$ is defined as feed direction angle γ. The expressions are as follows:

$$\varepsilon = \arccos\left(\frac{\mathbf{n}\cdot\mathbf{p}}{|\mathbf{n}||\mathbf{p}|}\right) \tag{1}$$

$$\begin{cases} \gamma = \arccos\left(\dfrac{\mathbf{s}\cdot\mathbf{f}}{|\mathbf{s}||\mathbf{f}|}\right) \\ \mathbf{s} = \mathbf{p}\times\mathbf{n} \end{cases} \tag{2}$$

The cutter axis leans relative to feed direction $\boldsymbol{f}$ in five-axis ball-end milling. The value range of feed direction angle γ is defined from 0 to π anti-clockwise.

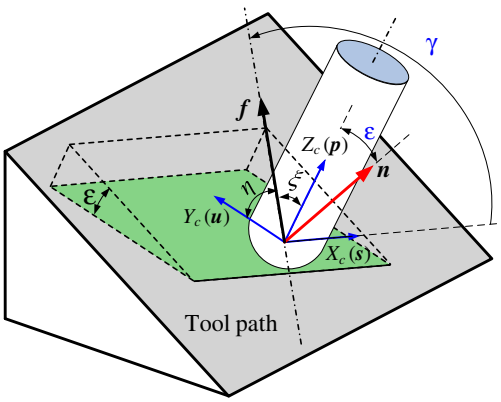

Fig. 2 Five-axis ball-end milling of inclined plane

Most of the cutting edges of ball-end mill are helical line with constant lead. The geometry of the ball-end mill with N teeth and radius R is shown in Fig. 3. k is the axial position angle measured from the negative z-axis to micro-cutting element. The cutting edge is discretized by axial position angle k. Because of the helical angle α, the helical lag angle φ of micro-cutting edge corresponding k at the radial position angle ψ of cutting edge j is

$$\varphi(k) = (\mathrm{j}-1)2\pi/N + (1-\cos k)\tan\alpha \tag{3}$$

The definitions of the relevant angles are shown in Fig. 3. The expression of cutting edge j is as follows:

$$\begin{cases} X_j = R\sin k\sin(\psi-\varphi(k)) \\ Y_j = R\sin k\cos(\psi-\varphi(k)) \\ Z_j = -R\cos k \end{cases} \tag{4}$$

The tangential force $\mathrm{d}F_{t,j}$, radial force $\mathrm{d}F_{r,j}$, and axial force $\mathrm{d}F_{a,j}$ acting on micro-cutting edge element k of edge j can be expressed with the Armarego's classical bevel cutting theory as

$$\begin{cases} \mathrm{d}F_{r,j}(\theta_j,k) = K_r t_n(\theta_j,k)\mathrm{d}b \\ \mathrm{d}F_{t,j}(\theta_j,k) = K_t t_n(\theta_j,k)\mathrm{d}b \\ \mathrm{d}F_{a,j}(\theta_j,k) = K_a t_n(\theta_j,k)\mathrm{d}b \end{cases} \tag{5}$$

where the width of micro-chip is

$$\mathrm{d}b = R\mathrm{d}k \tag{6}$$

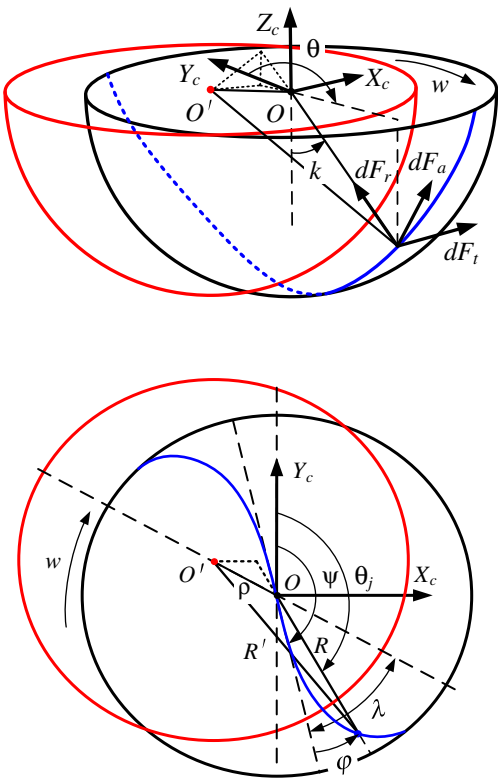

Fig. 3 Geometry and force analysis of cutting edge on ball-end mill

The instantaneous chip thickness can be divided into two parts (t_{n1} and t_{n2}), and it is the sum of t_{n1} and t_{n2}. In the five-axis ball-end milling, the feed direction relative to micro-cutting element is arbitrary. Based on Wei's theory [24], t_{n1} represents the projection of the feed on the normal direction of micro-cutting element k. The expression of t_{n1} is

$$\begin{aligned} t_{n1}(\theta_j,k) &= f_c\cos\gamma\sin k\sin\theta_j \\ &\quad + f_c\cos\eta\sin k\cos\theta_j - f_c\cos\xi\cos k \end{aligned} \tag{7}$$

where η is the angle between feed direction $\boldsymbol{f}$ and cutter coordinate Y_c-axis, while ξ is the angle between feed direction $\boldsymbol{f}$ and cutter coordinate Z_c-axis. Expressions are as follows:

$$\begin{aligned} \xi &= \arccos\left(\frac{\mathrm{p}\cdot\mathbf{f}}{|\mathrm{p}||\mathbf{f}|}\right) \\ \eta &= \arccos\left(\frac{\mathrm{u}\cdot\mathbf{f}}{|\mathrm{u}||\mathbf{f}|}\right) \end{aligned} \tag{8}$$

Due to manufacturing error, the cutter misalignment between the rotation center and geometric center changes the effective cutting radius of the cutter tooth and affects the effective undeformed chip thickness. Generalizing the definition of run-out parameters of flat-end mill [25] to the ball-end milling cutter, the distance between the geometric center O and the rotation center O′ is denoted as run-out distance ρ. The run-out angle λ defined in XOY plane is measured from line formed by geometric center and rotation center to the nearest tooth in the clockwise direction. As shown in Fig. 3, the effective cutting radius of micro-cutting element k on cutting edge j is

$$R'_j(\theta_j,k) = R + \rho\sin k\cos\left[\lambda-(\psi-\theta_j)-2(j-1)\pi/N\right] \tag{9}$$

Instantaneous chip thickness t_{n2} is the difference of the former and later effective cutting radius.

$$t_{n2}(\theta_j,k) = R'_{j+1}(\theta_j,k) - R'_j(\theta_j,k) \tag{10}$$

That is,

$$\begin{aligned} t_{n2}(\theta_j,k) &= -2\rho\sin k\sin(\pi/N)\sin(\lambda-\sigma) \\ \sigma &= \psi-\theta_j+(2j-3)\pi/N \end{aligned} \tag{11}$$

The direction of the micro-cutting edge milling force is related to the axial position angle k. The cutting forces in x, y, and z directions of cutter coordinate system obtained from coordinate transformation are

$$\begin{bmatrix} dF_{x,j}(\theta_j,k) \\ dF_{y,j}(\theta_j,k) \\ dF_{z,j}(\theta_j,k) \end{bmatrix} = \begin{bmatrix} -\cos\theta_j & -\sin k\sin\theta_j & \cos k\sin\theta_j \\ \sin\theta_j & -\sin k\cos\theta_j & \cos k\cos\theta_j \\ 0 & \cos k & \sin k \end{bmatrix} \begin{bmatrix} dF_{t,j}(\theta_j,k) \\ dF_{r,j}(\theta_j,k) \\ dF_{a,j}(\theta_j,k) \end{bmatrix} \tag{12}$$

Bring formula (5) into (12) and integrating axial position angle k along axis direction, the cutting force acted on cutter tooth j is evaluated:

$$\begin{bmatrix} F_{x,j}(\theta_j) \\ F_{y,j}(\theta_j) \\ F_{z,j}(\theta_j) \end{bmatrix} = \begin{bmatrix} \int_{k_d}^{k_u} dF_{x,j}(\theta_j,k) \\ \int_{k_d}^{k_u} dF_{y,j}(\theta_j,k) \\ \int_{k_d}^{k_u} dF_{z,j}(\theta_j,k) \end{bmatrix} = \begin{bmatrix} E_{11} & E_{12} & E_{13} \\ E_{21} & E_{22} & E_{23} \\ 0 & E_{32} & E_{33} \end{bmatrix} \begin{bmatrix} K_t \\ K_r \\ K_a \end{bmatrix} + \begin{bmatrix} G_{11} & G_{12} \\ G_{21} & G_{22} \\ G_{31} & G_{32} \end{bmatrix} \begin{bmatrix} \rho\sin\lambda \\ \rho\cos\lambda \end{bmatrix} \tag{13}$$

$$\begin{aligned} E_{11} &= -R\int_{k_d}^{k_u} \cos\theta_j t_{n1}(\theta_j,k)dk \\ E_{12} &= -R\int_{k_d}^{k_u} \sin k\sin\theta_j t_{n1}(\theta_j,k)dk \quad & E_{23} &= R\int_{k_d}^{k_u} \cos k\cos\theta_j t_{n1}(\theta_j,k)dk \\ E_{13} &= R\int_{k_d}^{k_u} \cos k\sin\theta_j t_{n1}(\theta_j,k)dk \quad & E_{32} &= R\int_{k_d}^{k_u} \cos k t_{n1}(\theta_j,k)dk \\ E_{21} &= R\int_{k_d}^{k_u} \sin\theta_j t_{n1}(\theta_j,k)dk \quad & E_{33} &= R\int_{k_d}^{k_u} \sin k t_{n1}(\theta_j,k)dk \\ E_{22} &= -R\int_{k_d}^{k_u} \sin k\cos\theta_j t_{n1}(\theta_j,k)dk \end{aligned}$$

$$\begin{aligned} G_{i1} &= R\int_{k_d}^{k_u} H_i \cos\sigma(\theta_j,k)dk \\ G_{i2} &= -R\int_{k_d}^{k_u} H_i \sin\sigma(\theta_j,k)dk \end{aligned} \quad i = 1,2,3$$

$$\begin{aligned} H_1 &= 2\sin(\pi/N)\left[\sin k\cos\theta_j K_t + \sin^2 k\sin\theta_j K_r - 0.5\sin(2k)\sin\theta_j K_a\right] \\ H_2 &= -2\sin(\pi/N)\left[\sin k\sin\theta_j K_t - \sin^2 k\cos\theta_j K_r + 0.5\sin(2k)\cos\theta_j K_a\right] \\ H_3 &= -2\sin(\pi/N)\left[0.5\sin(2k)K_r + \sin^2 k K_a\right] \end{aligned}$$

In Eq. (13), the integral upper and lower bounds k_u, k_d depend on the engagement condition of each cutting edge. The milling forces of three directions in the cutter coordinate system are the sum of all the teeth:

$$\begin{bmatrix} F_{xc}(\psi) \\ F_{yc}(\psi) \\ F_{zc}(\psi) \end{bmatrix} = \begin{bmatrix} \sum_{j=1}^{N} F_{x,j}(\theta_j) \\ \sum_{j=1}^{N} F_{y,j}(\theta_j) \\ \sum_{j=1}^{N} F_{z,j}(\theta_j) \end{bmatrix} \tag{14}$$

3 CWE of five-axis milling on inclined plane

The schematic diagram of five-axis ball-end milling of inclined plane is shown as Fig. 4. The CWE is closed spherical geometry, which consists of three curves, AB, AC, and BC. AB is the intersection of the current cutter swept surface N and the plane perpendicular to the feed direction through the center of cutter hemisphere. It is also a spatial circular arc of R. AC is

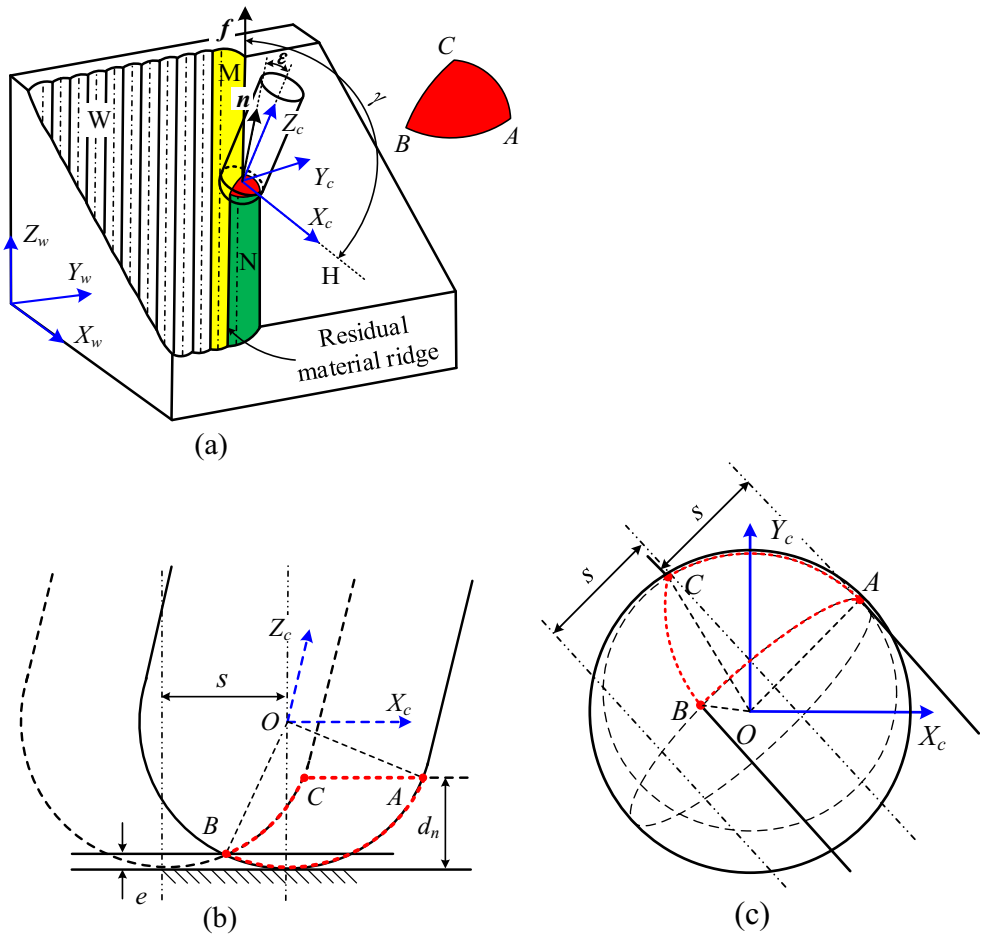

Fig. 4 CWE of five-axis ball-end milling of inclined plane. **a** Three-dimensional diagram. **b** View of feed direction. **c** Top view

the intersection of cutter hemisphere surface and the surface to be machined H, which is local spatial circular arc, while BC is the intersection of former swept surface M and hemisphere surface. The CWE is a part of the spherical surface, and the key is to determine the boundary curves. According to the analysis above, the analytic expressions of three boundary curves and intersection points of curves can be determined by the geometric method of intersection of spatial surfaces.

3.1 Boundary curves

The analytical expressions of swept surfaces M and N, surface remained to be machined H, hemispherical surface of ball-end mill, and spatial plane that is perpendicular to feed direction and cross through the original point O can be expressed in the cutter coordinate system O-$X_cY_cZ_c$ easily. The boundary curves can be obtained from equation set.

Boundary curve AB:

$$\begin{cases} x\cot\gamma + y\csc\varepsilon + z\sin\varepsilon = 0 \\ x^2 + y^2 + z^2 = R^2 \end{cases} \tag{15}$$

Boundary curve AC:

$$\begin{cases} y\sin\varepsilon - z\cos\varepsilon - R + d_n = 0 \\ x^2 + y^2 + z^2 = R^2 \end{cases} \tag{16}$$

Boundary curve BC:

$$\begin{cases} [x-(\pm s')\tan\gamma(\cot\varepsilon + \sin\varepsilon) + h\cot\gamma]^2 + (y \pm s'\cot\gamma + h\cos\varepsilon)^2 \\ \quad + (z \pm s' + h\sin\varepsilon)^2 = R^2 \\ x^2 + y^2 + z^2 = R^2 \end{cases} \tag{17}$$

where

$$h = 0.5\sin(2\gamma)\left[\left(\pm s'\right)\tan\gamma(\cot\varepsilon + \sin\varepsilon) - x\right] + \left(y \pm s'\cot\varepsilon\right)\cos\varepsilon + \left(z \pm s'\right)\sin\varepsilon \tag{18}$$

$$s' = s\left[(\cot\varepsilon + \sin\varepsilon)^2\tan^2\gamma + \cot^2\gamma + 1\right]^{-0.5}$$

where d_n is the normal depth of cut and s is the step distance. In Eq. (18), symbol − represents down milling, while symbol + denotes up milling.

The boundary curves of CWE intersect at the three points A, B, and C. Based on the theory that three surface intersect at one point, point A generates from the intersection of cutter sphere surface, surface to be machined H, and spatial plane that is perpendicular to feed direction and pass through the center of sphere; point B is the intersection of cutter sphere surface, former swept surface M, and spatial plane perpendicular to feed direction and pass through the center of sphere; point C is the intersection of cutter sphere surface, surface to be machined H, and former swept surface M. The expressions are

Point A

$$\begin{cases} x^2 + y^2 + z^2 = R^2 \\ y\sin\varepsilon - z\cos\varepsilon - R + d_n = 0 \\ x\cot\gamma + y\csc\varepsilon + z\sin\varepsilon = 0 \end{cases} \tag{19}$$

Point B:

$$\begin{cases} x^2 + y^2 + z^2 = R^2 \\ [x-(\pm s')\tan\gamma(\cot\varepsilon + \sin\varepsilon) + h\cot\gamma]^2 + (y \pm s'\cot\gamma + h\cos\varepsilon)^2 \\ \quad + (z \pm s' + h\sin\varepsilon)^2 = R^2 \\ x\cot\gamma + y\csc\varepsilon + z\sin\varepsilon = 0 \end{cases} \tag{20}$$

Point C:

$$\begin{cases} x^2 + y^2 + z^2 = R^2 \\ [x-(\pm s')\tan\gamma(\cot\varepsilon + \sin\varepsilon) + h\cot\gamma]^2 + (y \pm s'\cot\gamma + h\cos\varepsilon)^2 \\ \quad + (z \pm s' + h\sin\varepsilon)^2 = R^2 \\ y\sin\varepsilon - z\cos\varepsilon - R + d_n = 0 \end{cases} \tag{21}$$

The result of the intersections of A, B, and C is not unique in the space surface. In the case of down milling, the condition of the unique selection of the intersection coordinates is given in terms of the relative relation between the feed vector and the direction of the cutter axis:

$$x_A \geq 0; \quad \min(y_B); \quad \max(z_C). \tag{22}$$

The intersection of two surfaces is closed curve. In order to clearly show the CWE, only the boundary curve segment is preserved and the redundant curve segment needs to be discarded. The boundary curves of AB and BC are in the direction of feed side and under to be machined plane H; AC is located in the feed direction side and out the former swept surface. The judgment expressions are shown in (23) and (24), respectively.

$$\begin{cases} y\sin\varepsilon - z\cos\varepsilon - R + d_n \leq 0 \\ x\cot\gamma + y\csc\varepsilon + z\sin\varepsilon \geq 0 \end{cases} \tag{23}$$

$$\begin{cases} \left[x-\left(\pm s'\right)\tan\gamma(\cot\varepsilon + \sin\varepsilon) + h\cot\gamma\right]^2 + \left(y \pm s'\cot\gamma + h\cos\varepsilon\right)^2 \\ \quad + \left(z \pm s' + h\sin\varepsilon\right)^2 \geq R^2 \\ x\cot\gamma + y\csc\varepsilon + z\sin\varepsilon \geq 0 \end{cases} \tag{23}$$

As shown in Fig. 4b, the scallop height of the machined surface W is

$$e = \left(R - \sqrt{R^2 - (s/2)^2}\right) \tag{24}$$

4 ICCE of five-axis milling of inclined plane

The ICCE defines the scope of undeformed chip thickness, which reflects the condition of cutting edge involved in cutting at arbitrary time. The micro-cutting force exists only when the micro-cutting edge is in the CWE. This section obtains ICCE by intersecting cutting edge and CWE based on the established CWE model.

As shown in Fig. 5, the cutting edge curve 1 intersects the boundary curves BC and AB; the cutting edge curve 2 intersects the boundary curves AC and AB; the cutting edge curve 3 intersects the boundary curves BC and AC. In the combination of different ball-end mill geometry, feed direction, and machining parameters, there exist the intersections of cutting edge curves 4 and 5 with the CWE boundary curves. There are two intersection points between the cutting edge curve and the boundary curves, that is, the upper boundary point k_u and the lower boundary point k_d.

Based on boundary curve analytical expression, it can be found that boundary curve AB is monotonous along the X_c axis. When the feed direction angle γ is acute angle, the boundary curve BC is monotonous along X_c axis and AC is monotonous along the Z_c axis. When the feed direction angle γ is obtuse angle, boundary curve BC is monotonous along the Z_c axis and AC is monotonous along X_c axis. The boundary curves are discretized along the monotonic interval, and the boundary elements are the known spatial discrete point in the cutter coordinate system. When the degree of discretization is high enough, the nearest two points to the edge curve are the upper and lower points of the ICCE. Take the cutting edge 1 as an example, the boundary elements P_{bc} and P_{ab} are the upper and lower bounds of the ICCE respectively. The criteria conditions are expressed as follows:

$$\Delta e_{Pxz} = x_P - \sqrt{R^2 - z_P^2}\sin(\psi - (1 + z_P/R)\tan\alpha) \tag{25}$$

$$\Delta e_{Pyz} = y_P - \sqrt{R^2 - z_P^2}\cos(\psi - (1 + z_P/R)\tan\alpha) \tag{26}$$

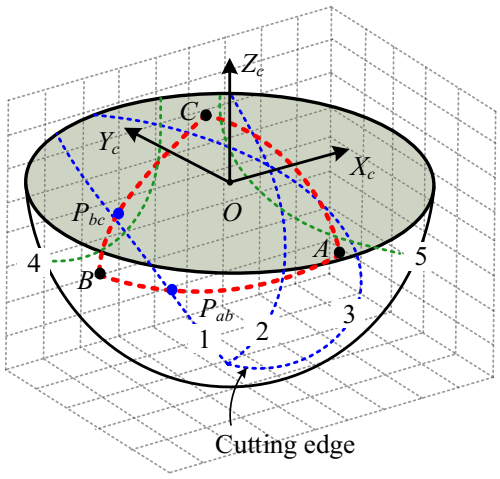

Fig. 5 ICCE of five-axis ball-end milling of inclined plane

$$\Delta e_P = \sqrt{\Delta e_{Pxz}{}^2 + \Delta e_{Pxz}{}^2} \le \Delta e \quad (\Delta e \ge \Delta e_p) \tag{27}$$

Δe_{Pxz} and Δe_{Pyz} represent spatial position distance from the boundary element coordinate P to cutting edge along the direction of X_c axis and Y_c, respectively. When the norm of Δe_{Pxz} and Δe_{Pyz} is less than the setting errors, the point P is regarded as one of boundary points of ICCE. It is noted that the setting error Δe should not less than half of the discrete distance Δe_P of CWE boundary elements.

Thus, the boundary element is searched and calculated one by one, and the upper and lower bounds of the ICCE can be found. The relationship between the coordinate of the boundary point and the axial position angle k is

$$k = \arccos(z/(-R)) \tag{28}$$

The ICCE of jth cutting edge is obtained based on this algorithm. The ICCE of adjacent edge can be determined by increasing cutter rotation position angle ψ $2\pi/N$.

5 Identification model of cutting force coefficients and run-out parameters

In order to obtain the instantaneous cutting force conveniently, and simplify the cutting force coefficient identification model, it is necessary to ensure the workpiece is cut by single tooth, that is, in any cutter rotation angle, there is only a group of upper and lower points k_u and k_d of ICCE. It can be identified by ICCE algorithm easily as Fig. 8b.

5.1 Cutting force coefficient identification

According to Kline's theory, the cutter run-out does not affect the average cutting force. From formula (10), it can be obtained that the average chip thickness of N teeth is constant and independent of the cutter run-out. Accordingly, formula (13) can be deformed into

$$\begin{bmatrix} \overline{F_{xc}(\psi)} \\ \overline{F_{yc}(\psi)} \\ \overline{F_{zc}(\psi)} \end{bmatrix} = \begin{bmatrix} E_{11} & E_{12} & E_{13} \\ E_{21} & E_{22} & E_{23} \\ 0 & E_{32} & E_{33} \end{bmatrix} \begin{bmatrix} K_t \\ K_r \\ K_a \end{bmatrix} \tag{29}$$

Instantaneous average milling forces are obtained from experiments. Taken the X_c-axis force in Fig. 6 as an example, the average milling force at cutter rotation location angle ψ and $\psi + 2\pi/N$ are not influenced by run-out.

$$\overline{F_{xc}(\psi)} = \frac{1}{N}\sum_{j=1}^{N} F_{x,j}(\psi) \tag{30}$$

The cutting force coefficients are unknown variables in formula (29), the method of undetermined coefficients is used

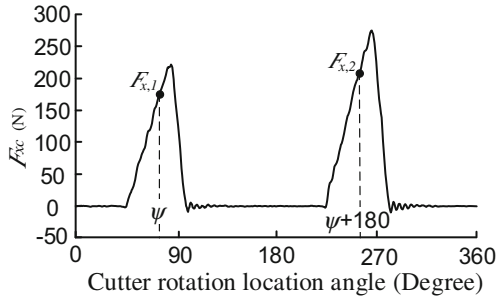

Fig. 6 Measured instantaneous milling force

to calibrate coefficients at arbitrary instantaneous time. The coefficients correspond to a certain undeformed chip thickness and ICCE. Cutting force coefficients are relative to the axial position angle k and the thickness of the chip layer t_n. A series of experiments are performed to obtain the instantaneous cutting force coefficients. Whereafter, the coefficients corresponding average axial position angle k' of ICCE and average chip thickness t_n' of ICCE at arbitrary time as variables are fitted as surface. Then, the instantaneous cutting force coefficient databases are obtained. $k'$and t_n' are defined as follows:

$$t_n^{'} = \int_{k_d}^{k_u} t_{n1}(\theta_j, k)/(k_u - k_d) \tag{31}$$

$$k^{'} = (k_u - k_d)/2 \tag{32}$$

5.2 Identification of cutter run-out parameters

Cutter run-out belongs to the geometric error and has nothing to do with the influence of machining parameters. Cutter run-out affects the amplitude of milling force waveform of each tooth. Whereupon the run-out parameters ρ and λ can be evaluated using milling force by inverse calculation. Bring formula (29) into the formula (13):

$$\begin{bmatrix} F_{xc}(\psi) - \overline{F_{xc}(\psi)} \\ F_{yc}(\psi) - \overline{F_{yc}(\psi)} \\ F_{zc}(\psi) - \overline{F_{zc}(\psi)} \end{bmatrix} = \begin{bmatrix} G_{11} & G_{12} \\ G_{21} & G_{22} \\ G_{31} & G_{32} \end{bmatrix} \begin{bmatrix} \rho\sin\lambda \\ \rho\cos\lambda \end{bmatrix} \tag{33}$$

where instantaneous cutting force $F_{xc}(\psi + 2\pi/N)$ can replace instantaneous cutting force $F_{xc}(\psi)$. In order to reduce the calculation error, the large amplitude and smooth waveform in X_c-axis of cutter coordinate system is selected to obtain the instantaneous cutting force and instantaneous average cutting force. When arranged the processing parameters of experiments, the difference between the minimum and maximum peak values of the tooth force waveform should be less than 50% of the latter [26]. Formula (33) can be simplified as

$$F = Q \begin{bmatrix} \rho\sin\lambda \\ \rho\cos\lambda \end{bmatrix} \tag{34}$$

ρ and λ as unknown variables, the equations are established through the method of undetermined coefficients. The maximum force at cutter rotation position angle $\psi_{\max}$ and other cutting force at ψ_l are chosen to establish equation set. The square of difference of predicted force and measured force are summed up; whereafter, the parameters corresponding to minimum value are chosen as the optimal cutter run-out parameters ρ and λ. The expressions of ρ and λ are

$$F = \begin{bmatrix} F_{xc}(\psi_{\max}) - \overline{F_{xc}(\psi_{\max})} \\ F_{xc}(\psi_l) - \overline{F_{xc}(\psi_l)} \end{bmatrix}$$

$$Q = \begin{bmatrix} G_{11}(\psi_{\max}) & G_{12}(\psi_{\max}) \\ G_{11}(\psi_l) & G_{12}(\psi_l) \end{bmatrix}$$

The matrix to solve run-out parameters is

$$\begin{bmatrix} \rho\sin\lambda \\ \rho\cos\lambda \end{bmatrix} = Q^{-1} F \tag{35}$$

6 Experiments and simulations

Five-axis machining that cutter axis has arbitrary relationship related to machined surface can be regarded as the five-axis machining of horizontal workpiece. This section arranges the

Fig. 7 CWE experiment and measured device. **a** Five-axis inclined plane milling. **b** Digital imaging tool microscope

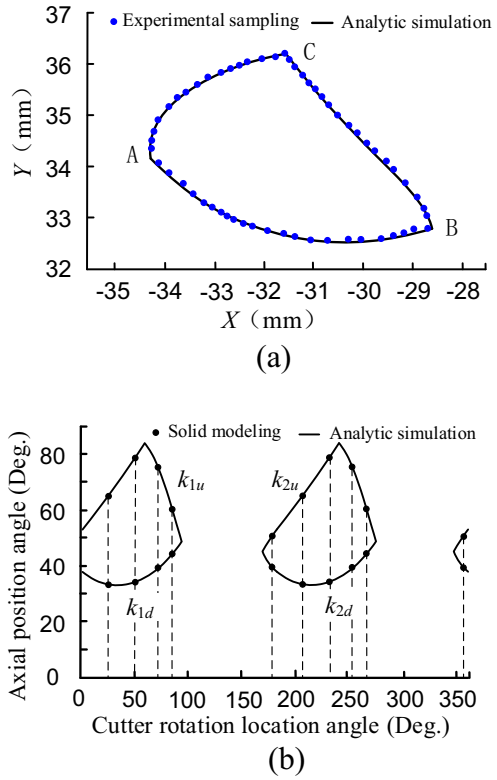

Fig. 8 Experiment and simulation results of CWE and ICCE. **a** CWE. **b** ICCE

experiments and simulations of the CWE and ICCE, as well as a series of experiments of five-axis milling of horizontal plane to verify the effectiveness of force coefficients and run-out parameter identification model.

6.1 CWE experiments and ICCE simulations

The down-milling experiment is shown in Fig. 7a; the size of workpiece is 80 mm × 70 mm × 5 1mm. The material is 45 steel. The angle between inclined plane and horizontal plane is 28°. A 10-mm diameter, 30° helical angle,

Table 1 Experimental parameters for coefficient identification

Cutter	ε (degree)	f (mm/min)
1	5 ~ 60 ($\Delta\varepsilon = 5°$)	150
2	5 ~ 60° ($\Delta\varepsilon = 5°$)	160

cemented carbide-coated ball-end mill with two right-hand flutes was used to cut. The step distance, normal depth of cut, inclination angle, and feed direction angle are 3 mm, 2 mm, 36°, and 85°, respectively. The left rear corner of top surface of the workpiece is the origin of the coordinate system. Tool path was generated by the stream-driven module of Unigraphics programming, NX. The experiment was carried out in DMU60 monoBLOCK, a five-axis CNC center.

The CWE obtained from experiment was placed under the VTM-3020F digital image tool microscope, and the view direction is shown in Fig. 7b. The left front corner of the top plane was set as origin of measurement. The results of sampling points of the boundary curves from experiment and the boundary curves from analytic simulation are shown in Fig. 8a. CWE based on analytical model presented in this paper agrees well with experiment result. Curve AB exists deviation slightly. The main reason is the smooth connection of the ball-end mill and current swept surface, which leads to unobvious intersection. Considering the cutter setting error, the measurement error, and the conversion error between the measuring datum and the machining datum, the experiment proves the effectiveness of the analytical model of the CWE.

Based on the ICCE algorithm proposed in this paper, for specific machining parameters of the abovementioned experiment, the upper and lower boundaries of ICCE at arbitrary radial position angle are shown as solid lines in Fig. 8b. Based on the solid method of Unigraphics NX modeling module, the cutter and workpiece at the instantaneous cutter point are modeled. Then, cutting edge is added at the

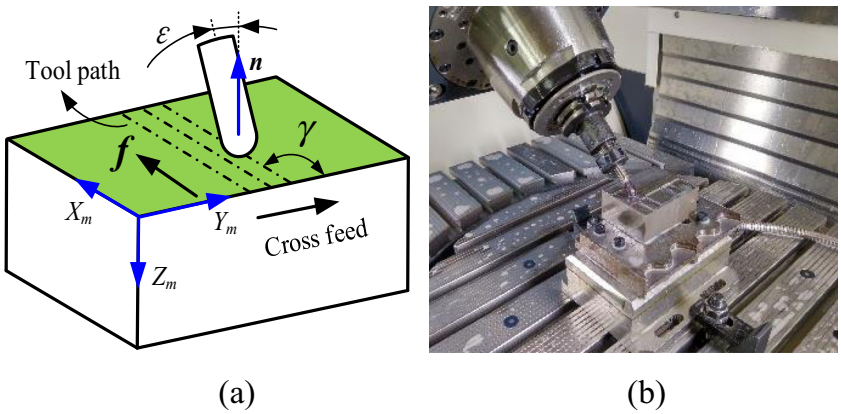

Fig. 9 Five-axis ball-end milling. **a** Schematic diagram. **b** Processing diagram

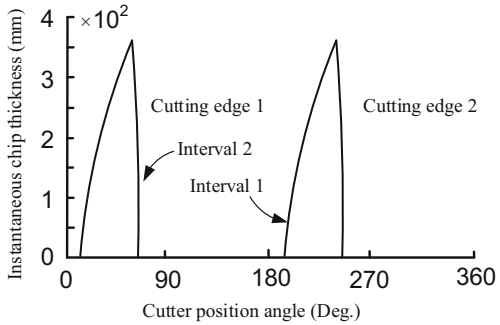

Fig. 10 Instantaneous average chip thickness

radial position angle of 25°, 50°, 70°, 85°, 175°, 205°, 235°, 255°, 265°, and 355°. Thereafter, the upper and lower boundaries of ICCE are obtained by intersection operation. The results show that the ICCE from the two methods match well, which demonstrates the effectiveness of analytical ICCE algorithm of five-axis ball-end milling of inclined plane.

6.2 Cutting experiments

The milling experiments schematic diagram and processing diagram are shown in Fig. 9. Workpiece was about 80 mm × 60 mm × 35 mm, 45 steel. Ten-millimeter diameter, 30° helix angle carbide-coated cutter 1 with one flute and cutter 2 with two flutes were used to cut. The single-tooth cutter is used to verify the identification of cutting force coefficients, and the double-teeth cutter can simultaneously verify the correctness of cutting force coefficients and cutter run-out parameters. In order to avoid machining chatter, the length of cutter suspension should be minimized under the premise of non-interference. Unigraphics NX machining module generated tool path. The experiments were performed on five-axis linkage machining center DMU60 monoBLOCK. The cutting forces were acquired by three-way piezoelectric quartz force sensor YDCB-III05, acquisition instrument INV3018A, and data processing system DSAP V10.01.

The cutting force coefficients and the cutter run-out parameters identification need to obtain cutting force data corresponding to different axial position angle and different instantaneous chip thickness. The spindle speed, depth of cut, and step distance are 500 r/min, 1 mm, and 1 mm, respectively. For facilitating the analysis, 12 groups of down-milling experiments with feeding direction angle 90° were carried for cutter 1 and cutter 2. The inclination angle and feed rate are shown in Table 1.

Three-way milling forces obtained from dynamometer coordinate system $O\text{-}X_mY_mZ_m$ are transformed into the cutter coordinate system $O\text{-}X_cY_cZ_c$:

$$\begin{cases} F_{xc} = F_{ym} \\ F_{yc} = F_{xm}\cos\varepsilon + F_{zm}\sin\varepsilon \\ F_{zc} = F_{xm}\sin\varepsilon - F_{zm}\cos\varepsilon \end{cases} \tag{36}$$

The changing trend of the instantaneous average chip thickness t_n' is consistent with the trend of the milling force. The thicker the t_n' is, the larger the milling force is, and t_n' comes to the top with F_{xc} at the same time. Take the cutter 2 and the inclination angle 60° as an example, bringing parameters into formula (31), instantaneous average chip thickness t_n' is evaluated as shown in Fig. 10.

The cutting interval 1 accounts for the majority of the cutting process. In order to obtain monotonous sampling data, five instantaneous radial position angles are selected averagely in interval 1, which includes the radial position angle corresponding to the maximum instantaneous chip thickness. Bring axial position angle k' obtained from formula (32) into formula (29), and then the three-way cutting force coefficients corresponding to the chip layer thickness t_n' and axial position angle k' are evaluated. The 5 × 12 sampling points coefficients are used to fit the surface based on formula (37) with curve fitting tool of MATLAB. Take the cutter 2 as an example, the polynomial coefficients of tangential coefficient K_t, the radial coefficient K_r, and axial coefficient K_a are shown in Table 2. The fitting surfaces are shown in Fig. 11.

Table 2 The polynomial coefficients of K_t, K_r, K_a

Coefficients	P_0	P_1	P_2	P_3	P_4	P_5	P_6
K_t	-1.46×10^4	2.8×10^4	8.46×10^5	-2.73×10^4	-2.04×10^6	-1.11×10^7	1.09×10^4
K_r	-1.57×10^4	1.77×10^4	1.47×10^6	-4.99×10^4	2.04×10^5	-7.7×10^7	3.53×10^4
K_a	1.79×10^3	-1.96×10^3	-9.54×10^4	-2.73×10^3	2.7×10^5	-1.13×10^5	2.84×10^3

Coefficients	P_7	P_8	P_9	P_{10}	P_{11}	P_{12}	P_{13}
K_t	1.15×10^6	4.43×10^7	-3.67×10^8	-3.83×10^5	-4.53×10^6	-4.33×10^8	8.67×10^9
K_r	3.82×10^5	-8.5×10^6	1.77×10^9	-1.11×10^6	4×10^7	-6.65×10^8	-1.03×10^{10}
K_a	-5.82×10^3	-6.97×10^6	1.01×10^8	-7.11×10^4	1.78×10^6	4.86×10^7	-1.93×10^9

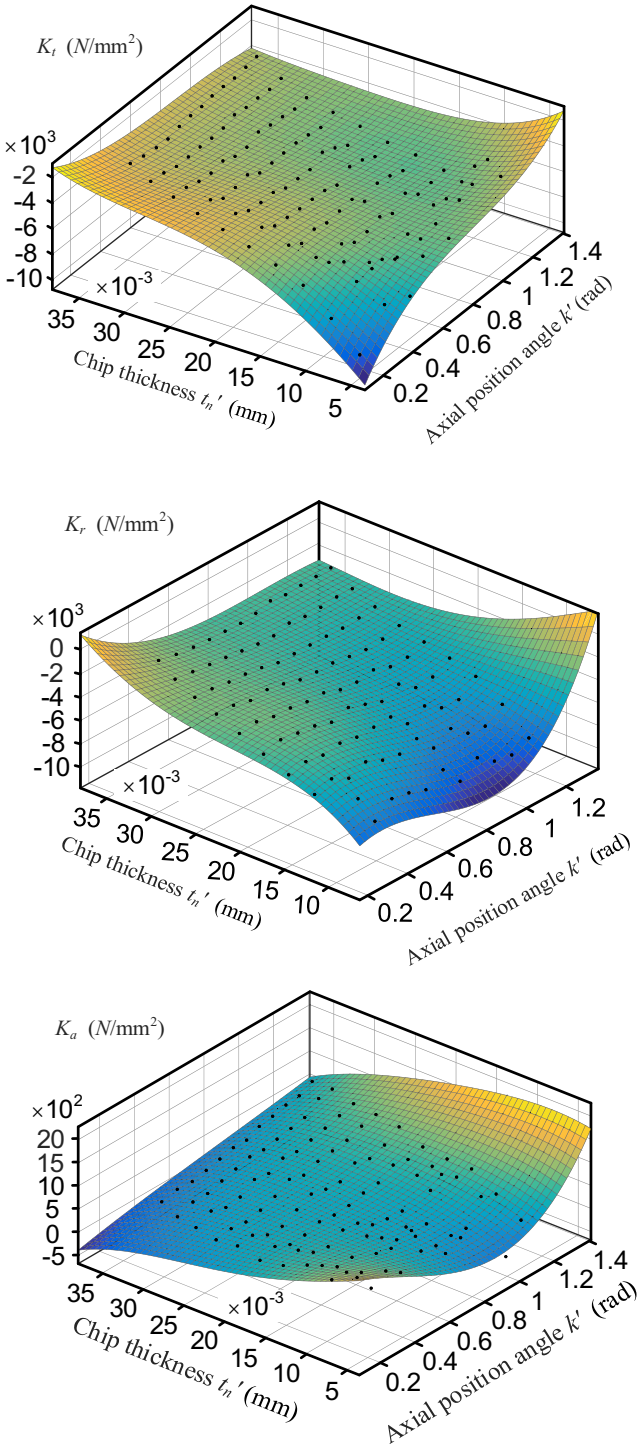

Fig. 11 Fitting surface of cutting force coefficients

$$K_v = p_0 + p_1x + p_2x^2 + p_3x^3 + p_4y + p_5y^2 + p_6y^3 + p_7y^4 + p_8xy + p_9x^2y + p_{10}xy^2 + p_{11}x^3y + p_{12}x^2y^2 + p_{13}xy^3 \quad \left(v = t, r, a; \quad x = k', y = t_n'\right) \tag{37}$$

Table 3 Experimental parameters for coefficients validation

Test	cutter	s(mm)	d_n (mm)	ε (degree)	f_z(mm/z)
1	1	1	1	60	0.3
2	1	1	1	5	0.3
3	1	0.5	1	30	0.3
4	1	1.5	1	30	0.3
5	1	1	0.5	30	0.3
6	1	1	1.5	30	0.3
7	1	1	1	15	0.18
8	1	1	1	40	0.24
9	2	1	1	55	0.16
10	2	1	1	20	0.16
11	2	1.5	1	30	0.1
12	2	1	1.8	30	0.1
13	2	1	1	45	0.06
14	2	1	1	5	0.12

Based on the run-out theory proposed in this paper, the run-out parameters of cutter 2 are obtained by bringing measured force and cutting force coefficients abovementioned into formula (35). As formulas (38) and (39) show, run-out parameters obtained from the experiments are different with the front incline of the cutter; that is, the run-out parameters corresponding to different axial position angles are different. The main reason is that different overcut occurs in milling and the cutter is not the ideal sphere.

$$\varepsilon = 55^o: \quad \rho = 0.01195\text{mm}; \quad \lambda = 106.78^o \tag{38}$$

$$\varepsilon = 55^o: \quad \rho = 0.01159\text{mm}; \quad \lambda = 96.83^o \tag{39}$$

$$\varepsilon = 10^o: \quad \rho = 0.01278\text{mm}; \quad \lambda = 91.25^o \tag{40}$$

In order to validate the applicability of the cutting force coefficients and the cutter run-out parameters, more than 200 tests for different cutting conditions were performed. Part of the tests are shown in Table 3.

The comparison of predicted milling force and measured force is shown in Fig. 12. The marked positions in the figure are relatively large, mainly concentrated on the right side of the force waveform with a small inclination angle. The reason is shown in Fig. 10. The model uses the interval 1 to identify the cutting force coefficients. The thickness of the material to be removed during the cutting process corresponding to section 1 and section 7 are getting thicker and getting thinner, respectively, so the cutting force coefficients of the two parts are not exactly the same. The predicted force is in good agreement with the measured force in the trend and amplitude, and the maximum error is less than 20% compared with the experimental results of the milling force with the variable depth, step distance, inclination angle, and feed per teeth, which prove the effectiveness of the milling force prediction model.

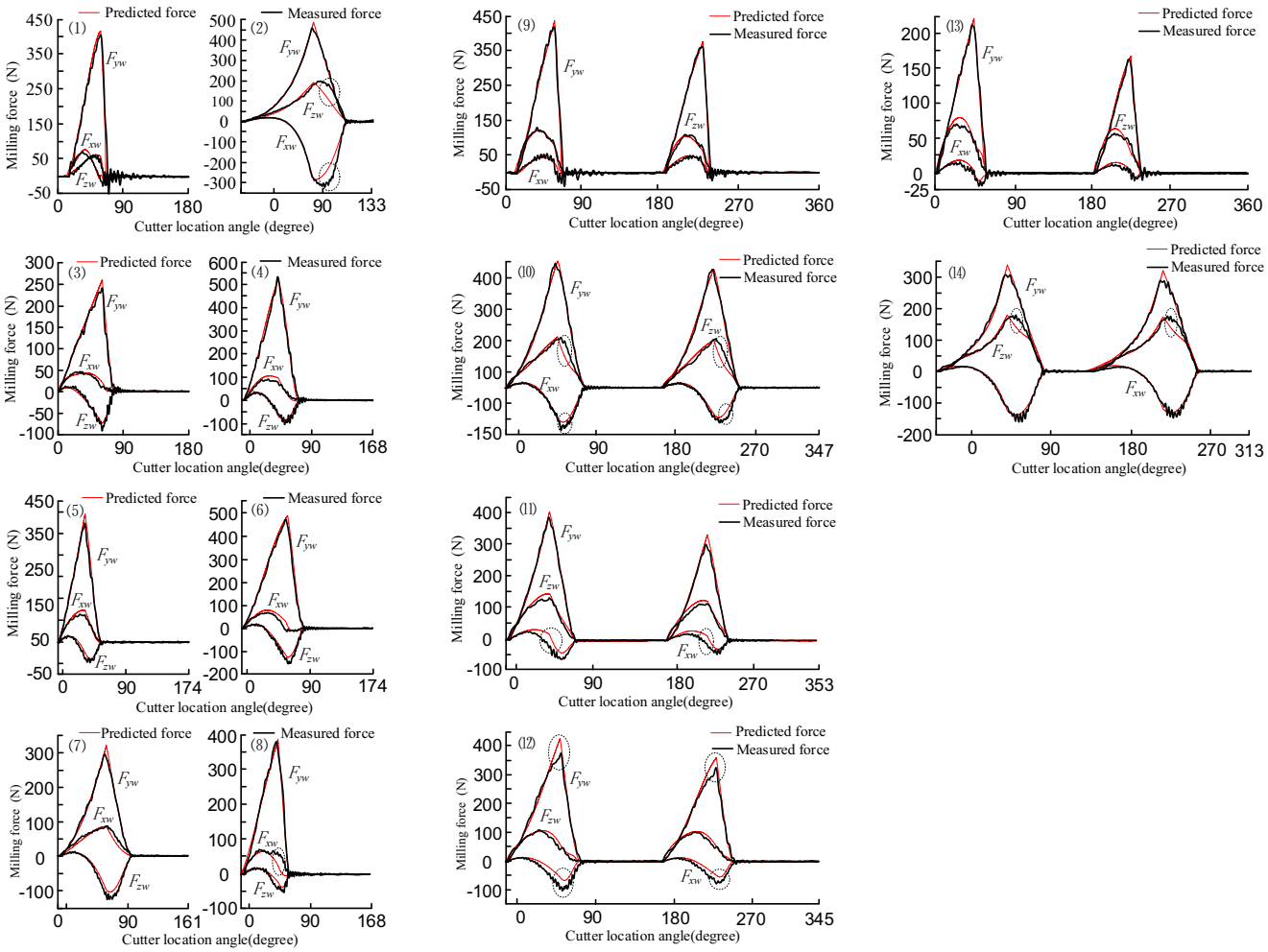

Fig. 12 Milling force prediction

7 Conclusions

The arbitrary relationships between the feed direction, the cutter axis vector, and the workpiece surface are parameterized in five-axis ball-end milling. The analytical expressions of swept surface by former tool path, machined surface, and spherical surface are deduced in cutter coordinate system. Then, the boundary curves of CWE and its inflection points are obtained by calculating intersection themselves.

Based on the obtained CWE, the boundary curves are discretized. The boundary elements are searched and judged one by one by defining the distance between the boundary element and the cutting edge curve. This proposed ICCE algorithm is suitable for five-axis ball-end mill.

A ball-end mill instantaneous chip thickness model is proposed considering cutter run-out and arbitrary feed direction. Combined with micro-cutting edge milling force theory and ICCE, the five-axis milling force model of ball-end mill is established.

Based on the method of undetermined coefficients, measured average instantaneous force of all teeth is brought into milling force model, then the cutting force coefficients corresponding to different instantaneous chip thickness and axial position angle can be solved. The cutting force coefficient identification model suitable for five-axis ball-end milling is established by fitting the discrete coefficients with surface. And then, the cutter run-out parameters are evaluated by combining measured instantaneous milling force of any tooth.

The experiment and simulation results of five-axis ball-end milling show that the CWE obtained from surface intersection is consistent well with the experimental results, and the ICCE by intersecting cutting edge and boundary curves of CWE is in good agreement with the ICCE based on the solid modeling method. A large number of milling experiments with different processing parameters show the effectiveness of the cutting force coefficients and the cutter run-out parameters identification model in the five-axis ball-end milling.

Funding information This research is supported by the Natural Science Foundation of Liaoning No. 201602174 and the Fundamental Research Funds for the Central Universities No. DUT17GF213.

References

1. Zhang X, Zhang J, Zhao WH (2016) A new method for cutting force prediction in peripheral milling of complex curved surface. Int J Adv Manuf Technol 86(1–4):117–128
2. Zhang DL, Mo R, Chang ZY, Sun HB, Li C (2016) A study of computing accuracy of calibrating cutting force coefficients and run-out parameters in flat-end milling. Int J Adv Manuf Technol 84(1–4):621–630
3. Guo D, Ren F, Sun Y (2010) An approach to modeling cutting forces in five-axis ball-end milling of curved geometries based on tool motion analysis. J Manuf Sci Eng 132(4):575–590
4. Fussell BK, Jerard RB, Hemmett JG (2000) Modeling of cutting geometry and forces for 5-axis sculptured surface machining. Comput Aided Des 35(4):333–346
5. Ferry W, Yip-Hoi D (2008) Cutter-workpiece engagement calculations by parallel slicing for five-axis flank milling of jet engine impellers. J Manuf Sci Eng 130(5):051011
6. Boz Y, Erdim H, Lazoglu I (2011) Modeling cutting forces for 5-axis machining of sculptured surfaces. Adv Mater Res 223:701–712
7. Ozturk E, Budak E (2005) Modeling of 5-axis milling forces. In: Proceedings of the eighth CIRP international workshop on modeling of machining operations, may 10–11, Chemnitz, Germany, 319–332
8. Ozturk B, Lazoglu I (2006) Machining of free-form surfaces. Part I: Analytical chip load. Int J Mach Tools Manuf 46(7):728–735
9. Sun YW, Guo Q (2011) Numerical simulation and prediction of cutting forces in five-axis milling processes with cutter run-out. Int J Mach Tools Manuf 51(10–11):806–815
10. Wei ZC, Wang MJ, Wang XW, Zhao DY (2017) A semi-analytical cutter workpiece engagement model for ball end milling of sculptured surface. J Mech Eng 53(1):198–205
11. Lee P, Altintaş Y (1996) Prediction of ball-end milling forces from orthogonal cutting data. Int J Mach Tools Manuf 36(9):1059–1072
12. Kim GM, Cho PJ, Chu CN (2000) Cutting force prediction of sculptured surface ball-end milling using Z-map. Int J Mach Tools Manuf 40(2):277–291
13. Wang JJJ, Huang CY (2004) A force-model-based approach to estimating cutter axis offset in ball end milling. Int J Adv Manuf Technol 24(11–12):910–918
14. Lamikiz A, Lacalle LNLD, Sanchez JA, Bravo U (2005) Calculation of the specific cutting coefficients and geometrical aspects in sculptured surface machining. Mach Sci Technol 9(3):411–436
15. Cao Q, Zhao J, Han S, Chen X (2012) Force coefficients identification considering inclination angle for ball-end finish milling. Precis Eng 36(2):252–260
16. Yao ZQ, Liang XG, Luo L, Hu J (2013) A chatter free calibration method for determining cutter runout and cutting force coefficients in ball-end milling. J Mater Process Technol 213(9):1575–1587
17. Ehsan Layegh KS, Lazoglu I (2014) A new identification method of specific cutting coefficients for ball end milling. Procedia CIRP 14(14):182–187
18. Wojciechowski S (2015) The estimation of cutting forces and specific force coefficients during finishing ball end milling of inclined surfaces. Int J Mach Tools Manuf 89:110–123
19. Li BC, Wang ZY, Wang GX, Wang WS (2016) Milling force coefficient identification of ball-end milling based on instantaneous milling forces. J Northeast Univ 37(5):678–682
20. Wan M, Ma CY, Zhang WH, Yang Y (2015) Study on the construction mechanism of stability lobes in milling process with multiple modes. Int J Adv Manuf Technol 79(1–4):589–603
21. Wan M, Ma CY, Feng J, Zhang WH (2016) Study of static and dynamic ploughing mechanisms by establishing generalized model with static milling forces. Int J Mech Sci 114:120–131
22. Wan M, Feng J, Ma YC, Zhang WH (2017) Identification of milling process damping using operational modal analysis. Int J Mach Tools Manuf 122:120–131
23. Wan M, Dang XB, Zhang WH, Yang Y (2018) Optimization and improvement of stable processing condition by attaching additional masses for milling of thin-walled workpiece. Mech Syst Signal Process 103:196–218
24. Wei ZC, Wang MJ, Cai YJ, Wang SF (2013) Prediction of cutting force in ball-end milling of sculptured surface suing improved Z-map. Int J Adv Manuf Technol 68:1167–1177
25. Yun WS, Cho DW (2000) An improved method for the determination of 3D cutting force coefficients and runout parameters in end milling. Int J Adv Manuf Technol 16(12):851–858
26. Wei ZC, Guo ML, Wang MJ, Li SQ, Liu SX (2018) Prediction of cutting force in five-axis flat-end milling. Int J Adv Manuf Technol 96(1–4):137–152